MATEC Web of Conferences **408**, 01027 (2025) https://doi.org/10.1051/matecconf/202540801027
IDDRG 2025

Determination of Kinematic Hardening Parameters in W-Temper Forming of 6082 Aluminum Alloy

Jemal Ebrahim Dessie[1*], *László* Rónai[2], and *Zsolt* Lukács[1]

[1]Institute of Materials Science and Technology, Faculty of Mechanical Engineering and Informatics, University of Miskolc, Miskolc, Egyetem út 1, 3515, Hungary
[2]Institute of Machine Tools and Mechatronics, Faculty of Mechanical Engineering and Informatics, University of Miskolc, Miskolc, Egyetem út 1, 3515, Hungary

Abstract. This study investigates the kinematic hardening behavior of 6082 aluminum alloy during W-temper forming, with a particular focus on the influence of transition time following W-temper heat treatment on key kinematic hardening parameters. Specifically, Young's Reduction Factor (γ), Young's Reduction Rate (χ), and Transient Softening Rate (K) were systematically analyzed. To achieve this, uniaxial tensile-compressive tests were conducted utilizing a newly developed anti-buckling fixture, while deformation characteristics were assessed through optical strain measurement. The experimental data were further processed and mathematically modeled in Scilab code using a point-by-point fitting approach. The results indicate that γ exhibits a marginal increase with prolonged transition time, signifying a more pronounced reduction in the elastic modulus over extended durations. Similarly, χ demonstrates an increasing trend with longer transition times, while the overall magnitude of the K exhibits a progressive increase with increasing strain. The material characterization methodology employed in this study demonstrates significant potential for enhancing the predictive accuracy of kinematic hardening behavior in sheet metal forming. These findings underscore the critical importance of optimizing heat treatment protocols to improve the manufacturability and performance of high-strength aluminum alloys.

Keywords: Kinematic hardening parameters; W-tempered 6082 aluminum alloy; Anti-buckling fixture; Point-by-point approach

1 Introduction

The final product's accuracy in sheet metal forming largely depends on the precision of the material hardening models [1-2]. Hardening models are classified as isotropic, kinematic, or combined. Isotropic models, commonly used in industry for their simplicity, describe the uniform expansion of the yield surface and effectively predict hardening in various materials [3-4]. Eggertsen et al. [5] analyzed cyclic phenomena captured by various hardening models and observed that increasing model complexity improved prediction accuracy. Kim et al. [6] demonstrated that a modified mixed Chaboche model effectively captured the Bauschinger and transient behavior in dual-phase materials. Similarly, Shi et al. [7] identified constitutive parameters for a combined isotropic-kinematic hardening model based on the Yoshida model. Gil et al. [8] further showed that a mixed hardening model provided significantly more precise geometric predictions for DP1000 components compared to a standard isotropic model.

Kinematic hardening laws offer more advanced modeling than isotropic models, allowing yield surfaces to translate while maintaining their shape and size. These models have gained attention for their ability to predict phenomena like the Bauschinger Effect [9]. The transient Bauschinger deformation involves early re-yielding and a gradual elastic-plastic transition with a rapid change in work hardening rate as illustrated in Fig. 1 [10-12]. In Fig. 1, ε_{rl} is linear reverse strain, and ε_{rn} is the nonlinear reverse strain.

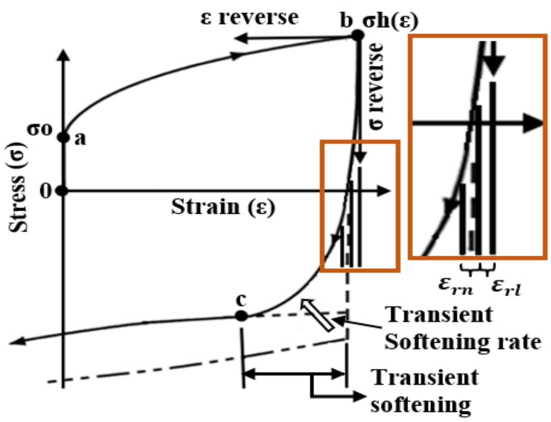

Fig. 1. The schematic tensile-compressive curve of sheet metal with Bauschinger effect description.

Analyzing the Bauschinger effect requires determining the stress-strain response under uniaxial tension-compression loading. However, conducting cyclic loading experiments on metal sheets is

* Corresponding author: metjemal@uni-miskolc.hu

challenging due to their susceptibility to buckling during compression.

Yoshida et al. [13] examined the cyclic behavior of mild and high-strength steel specimens, subjecting them to a maximum strain of approximately 8%, an unusually high level for such tests. Boger et al. [14] enhanced compression testing for thin sheet materials by implementing a laminated specimen system and a specialized apparatus to support the material during compression. Stoudt et al. [15] conducted similar research and successfully generated a compressive curve corresponding to a pre-strain of 4%. Kuwabara et al. [16] extended the strain range by integrating comb-shaped supports, further refined with male and female dies that slid against each other during compression. M. Härtel et al. [17] advanced Kuwabara et al.'s design by incorporating clamps for specimen fixation and four adjustable comb-shaped elements to limit out-of-plane deformation. Cao et al. [18] introduced a double-wedge setup applying lateral force to counteract buckling. Chang et al. [19] developed an in-plane tensile-compressive device using two T-shaped solid plates with fixed and movable ends to provide stable support during continuous tensile-compressive testing. Recent studies have extensively utilized tension-compression tests to examine the Bauschinger behavior of materials [20–24]. However, performing these tests remains challenging, particularly at high strain levels during compressive loading. Careful evaluation of the anti-buckling fixture's influence is essential, as it can significantly affect experimental data and compromise the reliability of the results.

This study applied a new anti-buckling fixture for uniaxial tension-compression testing, integrating the Vialux AutoGrid optical strain measurement system for precise, non-contact deformation tracking. To prevent buckling and ensure structural stability during cyclic loading, the specimen must be fully enclosed within an acrylic block. Figure 2 illustrates the testing procedure, where the fixture starts in its initial position (Fig. 2a) and testing begins from a pre-compressed state (Fig. 2b). The corresponding positions under tensile and compressive loads are shown in Fig. 2c and 2d. The experimental setup of the universal material testing machine configured with a new anti-buckling fixture, as illustrated in Fig. 3.

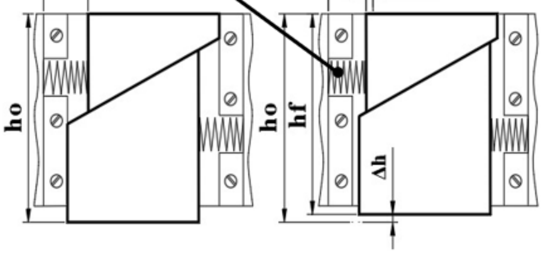

a)

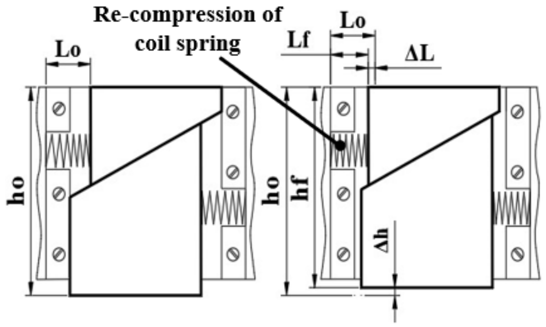

b)

Fig. 2. The testing procedure of the fixture, a) initial position of the fixture, b) pre-compression of acrylic blocks by a displacement change Δh and change in coil spring length Δh c) a position after applying the tensile load, d) a position after applying the compression load

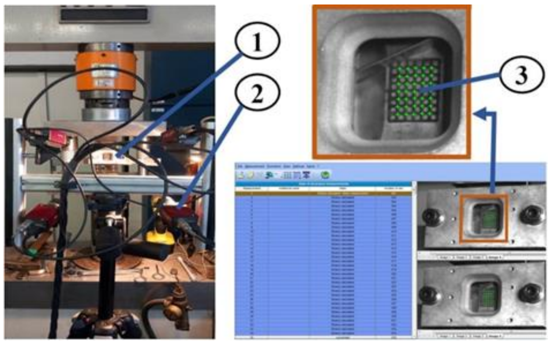

Fig. 3. Experimental setup (1-anti-buckling fixture, 2-CCD camera, 3-detected grid points in ViaLux code)

The developed fixture necessitated a compensation function to account for device-induced effects. To evaluate these effects, full-cycle tests were conducted using an undeformed specimen, enabling a comprehensive assessment of the fixture's influence on the measured response. Figure 4 illustrates the maximum, minimum, and average deviations observed in the force-displacement curve, incorporating data from repeated measurements to ensure reliability and accuracy.

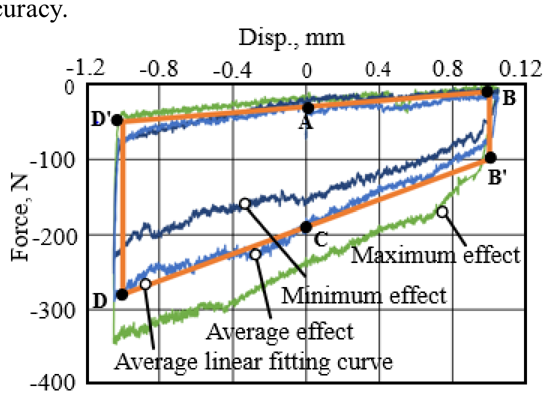

Fig. 4. The effect of the device on the displacement-force curve (line AB-tensile region; line B'C unloading region; line CD-compression region; and line D'A re-tensile region).

A linear fitting function was applied to the average effect to account for device-induced influences in the tension-compression test. The linear compensation model for the tension and re-tension regions is defined by Eq. (1a), while Eq. (1b) describes the compensation approach for the unloading and compression regions.

$$F = 20d - 30 \tag{1a}$$
$$F = 90d - 190 \tag{1b}$$

where F represents the force in (N) and d denotes the displacement in (mm).

This approach enhances the accuracy and reliability of measurements during testing. Figure 5 presents the force-displacement curve for the full-cycle monotonic tension-compression test, both before and after compensation for device-induced effects. While the device influence is negligible in the tensile and re-tensile regions, it has a pronounced impact during the unloading and compression phases.

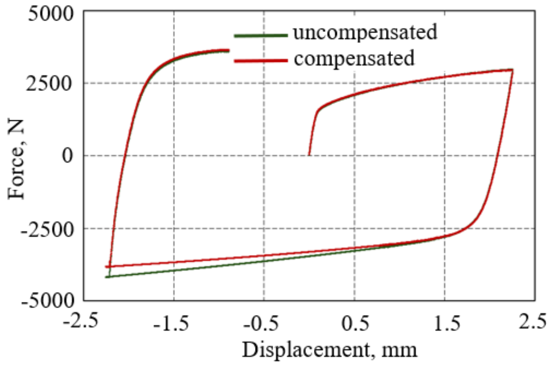

Fig. 5. Monotonic tension-compression test before and after compensation of the device effect.

This study investigates the key kinematic hardening parameters of AA6082 under cyclic loading during the W-temper forming process. Reverse stress-strain curves were fitted using a point-by-point approach in Scilab software, based on theoretical models implemented in the AutoForm numerical software. Furthermore, the influence of varying transition times after quenching on these parameters was analyzed.

2 Constitutive modeling of cyclic plastic deformation in AutoForm

During the reverse loading, specific hardening behaviors can be identified and grouped into four primary components: Young's reduction factor, Young's reduction rate, and transient softening rate [25-26]. Together, these phenomena are collectively referred to as the Bauschinger behavior of the material. A novel method has been developed and implemented in the AutoForm commercial FEM code to model the material kinematic hardening behavior, as it is described in Eq. (2) [11, 25]. This model accurately calculates Young's reduction factor and Young's reduction rate [27].

$$E_l = E_0\left(1 - \gamma\left(1 - \mathrm{e}^{-\chi P}\right)\right) \tag{2}$$

where E_0 is Young's modulus in GPa at zero plastic strain, E_l is the tangent modulus, which ordinarily falls off exponentially as a function of strain P, χ and γ are constants related to Young's as a function of deformation.

The Bauschinger effect, also referred to as transient softening, is quantitatively defined as the difference between the tensile flow stress at a specified forward strain and the compressive yield stress upon load reversal. This phenomenon reflects the material's tendency to exhibit reduced resistance to deformation in the reverse loading direction due to prior plastic deformation.

In AutoForm, the Bauschinger effect is characterized by the Transient Softening Rate (K), which is described as the sum of linear and non-linear reverse strain and mathematically modeled using Eq. (3) to approximate the hyperbolic function of the reverse stress-strain curve [25, 27].

$$\varepsilon_r = \varepsilon_{rl} + \varepsilon_{rn} = \frac{\sigma_r}{E_1(p)} + K \cdot \operatorname{arctanh}^2\left(\frac{\sigma_r}{2\sigma_h(p)}\right)^2 \tag{3}$$

where $\sigma_h(p)$ is accumulated plastic strain-dependent isotropic stress (see Fig. 1), σ_r is the reverse stress, ε_r is total reverse strain, ε_{rl} is linear reverse strain, and ε_{rn} is the nonlinear reverse strain.

3 Point-by-point analysis of kinematic hardening parameters

The calculation of the apparent elastic modulus at varying levels of deformation was performed by analyzing the slope of the unloading stress-strain curve over a specified stress range. There are two commonly applied methods to investigate it: (1) average Young's modulus (E_{av}) and (2) chord modulus.

E_{av} is defined as an average slope of the unloading stress-strain curve at four stress ranges: (1) $0.75\sigma_0 < \sigma < 0.95\sigma_0$, (2) $0.5\sigma_0 < \sigma < 0.95\sigma_0$, (3) $0.25\sigma_0 < \sigma < 0.95\sigma_0$ and (4) $0\sigma_0 < \sigma < 0.95\sigma_0$ [13][27].

In the chord modulus, the slope between the points at the maximum and minimum load of the unloading curve is considered. The elastic modulus during unloading was obtained by dividing the stress before unloading by the total reverse strain at zero stress, [28-30].

In AutoForm, there is an approximation module to estimate the transient softening rate (K). However, this approach provides only an approximate solution and requires additional numerical modeling of reverse stress to account for all relevant data points comprehensively. In this study, an alternative approach called the point-by-point method was applied.

The point-by-point method entails determining the parameters by evaluating all data points. A special purpose program is written in Scilab software for a series of measurements. The curve fitting method is based on the Least Squares Method (LSQ).

It is necessary to prepare the data in a .csv file, excluding the tensile stress section from the measurement data set. The first part of the program will search the positive stress values belonging to the unloading part to calculate the slope, which is the average elastic modulus for the given measurement using Eq. (4).

$$E_l(p) = \frac{\sum_{i=1}^{n-1}\left(\frac{\sigma_i - \sigma_{i+1}}{|\varepsilon_i - \varepsilon_{i+1}|}\right)}{n}, \tag{4}$$

This where ε_i, ε_{i+1} σ_i and σ_{i+1} are the i^{th} and $(i+1)^{\text{th}}$ strain and positive stress values from the imported data set, respectively. A for loop is setup to calculate $E_l(p)$. The number of data points is denoted by n.

Thereafter the data set is converted to the $\varepsilon_r - \sigma_r$ coordinate system. In order to use the LSQ technique on the measured data points for curve fitting, a definition of an error function is needed:

$$D = \varepsilon_r(\sigma_r) - \varepsilon_m, \tag{5}$$

where $\varepsilon_r(\sigma_r)$ is the reverse strain calculated by Eq. (3) in the function of the σ_r. ε_m is the measured strain value at each measurement point. In fact, the first part of the error function is the prediction of the model, while the second part is the measured, i.e., observed value. The technique minimizes the sum of the square of the deviations:

$$min\|D\|^2 = \sum_{i=1}^{n} D_i^2, \tag{6}$$

where n is the number of measurement points.

The isotropic hardening stress is determined from the data set as follows:

$$\sigma_h(p) = |\sigma^n|, \tag{7}$$

where σ^n is the last stress value defined in the original and not the reverse coordinate system.

4 Material characterization

Aluminum alloys, particularly the 6082 series, are extensively utilized in the automotive industry due to their high strength-to-weight ratio, corrosion resistance, and recyclability. Despite these advantageous mechanical properties, the 6082 alloy exhibits limited formability at room temperature. W-temper forming has been shown to significantly enhance formability, potentially enabling forming operations at room temperature. This process involves solution heat treatment, followed by rapid quenching and subsequent transit to the forming stage.

The W-temper forming process for 6082 aluminum alloys involves a solution heat treatment (SHT) at 525 °C [31], where the material is held at a high temperature long enough to fully dissolve alloying elements into the aluminum matrix. Notably, variations in Transition Time (TT), the interval between quenching and subsequent mechanical testing, can significantly influence microstructural evolution and kinematic hardening behavior. The temperature profile for the W-temper forming method used in this study is depicted in Fig. 6.

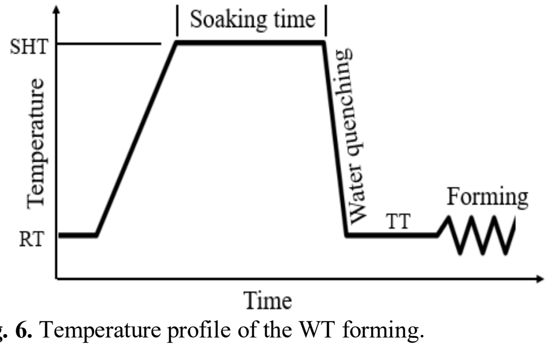

Fig. 6. Temperature profile of the WT forming.

In this study, a muffle laboratory furnace was utilized, and experimental observations confirmed that a heating duration of 30 minutes was necessary to attain a uniform temperature distribution at 525 °C. To assess the impact of TT on the material mechanical characteristics, tension-compression cyclic tests were performed at two distinct transfer times: 30 minutes and 120 minutes.

5 Results and discussion

This study focuses on examining how varying TT during the W-tempering process influences critical mechanical parameters, including Young's reduction factor (γ), Young's reduction rate (χ), and transient softening rate (K). In the subsequent sections, the effects of TT on the kinematic hardening parameters are comprehensively discussed.

The true stress-strain diagrams obtained from the tension-compression test at different deformation percentages for 30 and 120-minute TT are illustrated in Fig. 7. These diagrams highlight critical regions of reverse stress corresponding to various percentages of deformation for analyzing kinematic hardening parameters.

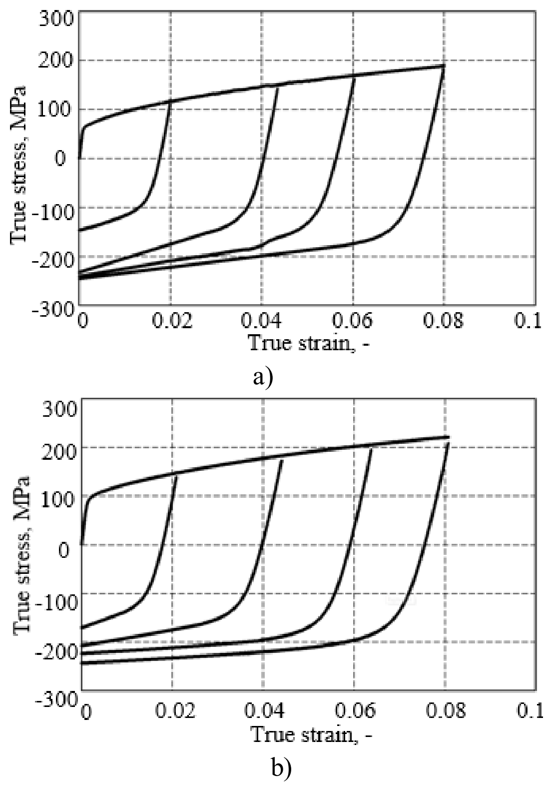

Fig. 7. Monotonic tension-compression test for W-tempered 6082 aluminum alloy: a) at 30 min TT, b) at 120 min TT.

5.1 Effect of transition time on the Young's reduction factor (γ) and Young's reduction rate (χ)

The degradation of the apparent elastic modulus as a function of deformation was systematically analyzed for each transition time. As depicted in Fig. 8, a distinct variation and a gradual decline in the elastic modulus were observed with increasing deformation for each TT, as computed using the point-by-point method. The parameters γ and χ were quantified through curve-fitting techniques applied to the experimental data, ensuring accurate characterization of the material's hardening behavior.

Table 1 presents the computed values of γ and χ for TT of 30 minutes and 120 minutes. The findings suggest that the γ values are slightly lower for the 30-minute TT; however, this difference is negligible when compared to the 120-minute TT. In contrast, the Young's reduction rate parameter (χ) exhibits a significant variation with prolonged TT, indicating a more pronounced reduction in Young's modulus during the unloading phase.

Determining Young's modulus is a challenging task and highly sensitive to the data selected for the calculation. The application of the point-by-point method, which allows for the evaluation of all data points within the unloading region, may offer a more comprehensive and precise assessment of Young's modulus degradation. However, validation is required through comparison with the average and chord modulus. This approach improves the overall reliability of computational modeling in material science research, as the computational method is supported by specialized software.

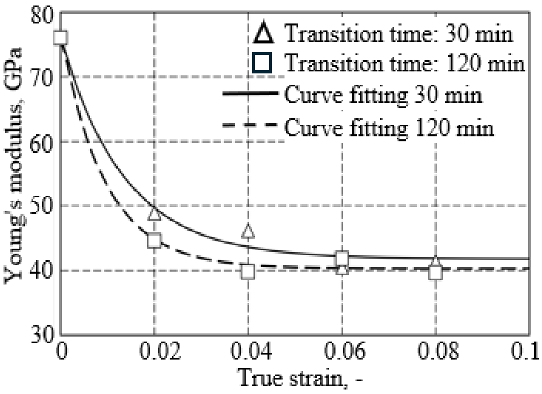

Fig. 8. Effect of TT on Young's modulus reduction as a function of strain.

Table 1. Effect of TT on Young's Reduction Factor (γ) and Young's Reduction Rate (χ)

Transition time (minutes)	Young's Reduction Factor (γ)	Young's Reduction Rate (χ)
30	0.45	73
120	0.47	103

5.2 Effect of transition time on the transient softening rate (K)

Furthermore, the Transient Softening Rate (K) was determined using the same point-by-point method outlined in the previous section using Eq. (3). The approximation module in AutoForm was also employed for comparative analysis. This dual-method approach enhances the reliability and robustness of the computed transient softening behavior, thereby facilitating a more comprehensive and accurate evaluation of the material's mechanical response.

The influence of TT on transient softening was systematically investigated at the same two distinct TT values discussed in the previous section. The experimental results, supported by point-by-point computational method, analyzed the relationship between TT and transient softening behavior, thereby enhancing the understanding of its impact on material performance.

As illustrated in Fig. 9 and Table 2, the Transient Softening Rate (K) shows an increasing trend with strain for specimens subjected to a transfer time of 30 minutes. Similarly, for specimens subjected to a transfer time of 120 minutes, the results indicate a comparable increasing trend in K with strain. However, the overall magnitude of K was slightly lower in the 120-minute TT condition compared to the 30-minute TT, suggesting that prolonged transition times result in a reduction in transient softening.

In general, this study observed that the Transient Softening Rate (K) increases as a function of strain, indicating that transient softening becomes more pronounced with increasing deformation. The computational methodology utilized in this study offers a robust mathematical framework for evaluating K. Furthermore, the comparison between the point-by-point approach and AutoForm approximations highlights the reliability and accuracy of the computational modeling of K in W-temper forming processes.

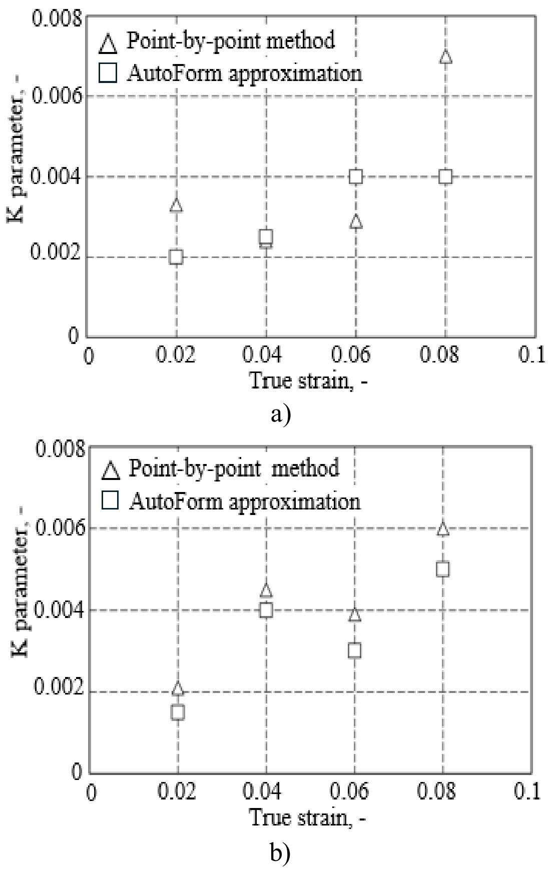

Fig. 9. Effect of TT on Transient Softening Rate (K) at various deformation levels a) at 30-minute TT, b) at 120-minute TT.

Table 2. Effect of TT on Transient Softening Rate (K) at various deformation levels

Strain ,-	K,-			
	30-min TT		120-min TT	
	Point-by-point	**AutoForm Approximation**	**Point-by-point**	**AutoForm Approximation**
0.02	0.00333	0.002	0.0021	0.0015
0.04	0.0024	0.0025	0.0045	0.004
0.06	0.003	0.004	0.0039	0.003
0.08	0.007	0.004	0.006	0.005

6 Conclusions

This study presents a comprehensive evaluation of the kinematic hardening behavior of W-tempered AA 6082 high-strength aluminum alloy, with a particular focus on the influence of transition time during the heat treatment process. The computational approach employed for reverse stress-strain curve fitting is crucial in the accurate assessment of kinematic hardening parameters. Extending the transition time from 30 minutes to 120 minutes has a minimal impact on the Young's reduction factor (γ). However, the Young's reduction rate parameter (χ) exhibits a significant change. The study investigates the effect of stress-strain cyclic loops and transition time on the transient softening rate during the W-temper forming of AA6082 aluminum alloy. The results indicate that as the strain amplitude increases, the transient softening rate (K) also increases. The transient softening rate at the 120-minute transition time was slightly lower than that observed at the 30-minute transition time.

References

1. F. Yoshida, T. Uemori, Int. J. Plast., **18**, 661 (2002)
2. E. Silvestre, J. Mendiguren, E. S. de Argandoña, L. Galdos, 14th International Metal Forming Conference, Krakow, 1295 (2012)
3. E. Silvestre, J. Mendiguren, L. Galdos, E. S. de Argandoña, Int. J. Mech. Sci., **101**, 10 (2015)
4. S. Bouvier, J. L. Alves, M. C. Oliveira, L. F. Menezes, Comput. Mater. Sci., **32**, 301 (2005)
5. P. A. Eggertsen, K. Mattiasson, Int. J. Mech. Sci., **52**, 804 (2010)
6. J. H. Kim, D. Kim, F. Barlat, M. G. Lee, Mater. Sci. Eng. A, **539**, 259 (2012)
7. M. F. Shi, L. Zhang, X. Zhu, J. Phys. Conf. Ser., **734**, p. 032118 (2016)
8. I. Gil, E. Silvestre, L. Galdos, J. Mendiguren, E. Sáenz de Argandoña, E. Hug, AIP Conf. Proc., **1769**, (2016)
9. G. B. Broggiato, F. Campana, L. Cortese, Meccanica, **43**, 115 (2008)
10. Y. Xiang, J. J. Vlassak, Scr. Mater., **53**, 177 (2005)
11. W. Kubli, A. Krasovskyy, M. Sester, M. Int. J. Mater. Form., **1**, 145 (2008)
12. X. Lemoine, A. Aouafi, Int. J. Mater. Form., **1**, 241 (2008)
13. F. Yoshida, T. Uemori, K. Fujiwara, Int. J. Plast., **18**, 633 (2002)
14. R. K. Boger, R. H. Wagoner, F. Barlat, M. Lee, K. Chung, Int. J. Plast., **21**, 2319 (2005)
15. M. R. Stoudt, L. E. Levine, L. Ma, Exp. Mech., **57**, 155 (2017)
16. T. Kuwabara, Y. Kumano, J. Ziegelheim, I. Kurosaki, Int. J. Plast., **25**, 1759 (2009)
17. M. Härtel, C. Illgen, M. F. Wagner, IOP Conf. Ser. Mater. Sci. Eng., **118**, p. 012018 (2016). IOP Publishing.
18. J. Cao, W. Lee, H. S. Cheng, M. Seniw, H. Wang, K. Chung, Int. J. Plast., **25**, 942 (2009)
19. Y. Chang, B. T. Wang, X. D. Li, C. Y. Wang, K. M. Zhao, H. Dong, J. Mater. Process. Technol., **278**, 116540 (2020)
20. K. Yu, H. Choi, J. Ha, J. W. Yoon, Int. J. Mater. Form., **16**, 16 (2023)
21. J. Min, N. Guo, Y. Hou, K. Jiang, X. Chen, J. E. Carsley, J. Lin, Int. J. Mater. Form., **14**, 435 (2021)
22. Y. Hou, J. Min, J. Lin, Z. Liu, J. E. Carsley, T. B. Stoughton, Procedia Eng., **207**, 173 (2017)
23. G. Joo, H. Huh, J. Kwon, J. Mater. Process. Technol., **270**, 365 (2019)
24. J. Lin, Y. Hou, J. Min, H. Tang, J. E. Carsley, T. B. Stoughton, Int. J. Mater. Form., **13**, 1 (2020)
25. D. Banabic, Sheet metal forming processes, Springer Science & Business Media (2010)
26. N. Han, W. Ma, X. Zheng, J. Yang, 3rd International Conference on Control, Automation and Artificial Intelligence, 214 (2018)
27. J. E. Dessie, Z. Lukacs, Z. Pollack Periodica, **19**, 54 (2024)
28. S. F. Lajarin, C. P. Nikhare, P. V. P. Marcondes, J. Braz. Soc. Mech. Sci. Eng., 40, 1 (2018)
29. A. Kupke, P. D. Hodgson, M. Weiss, J. Mater. Eng. Perform., 26, 3387 (2017)
30. R. Cobo Molina, M. Pla, R. Hernández Rossi, J. A. Benito Páramo, IDDRG 2009, 109 (2009)
31. M. S. Mohamed, A. D. Foster, J. Lin, D. S. Balint, T. A. Dean, IJMTM, **53**, 27 (2012)